CICE 2023 Rio de Janeiro - Brazil 11TH INTERNATIONAL CONFERENCE ON FRP COMPOSITES IN CIVIL ENGINEERING

ANALYTICAL PREDICTION OF FLEXURAL BEHAVIOUR OF RC SLABS STRENGTHENED WITH NON-PRESTRESSED AND PRESTRESSED CFRP STRIPS

Aloys Dushimimana, University of Minho, Portugal, aloysdushimimana@yahoo.fr
Luís Correia, University of Minho, Portugal, lcorreia@civil.uminho.pt
Ricardo Cruz, University of Minho, Portugal, a51314@alumni.uminho.pt
Susana Cabral-Fonseca, Laboratório Nacional de Engenharia Civil, Portugal, sbravo@lnec.pt
João Miguel Pereira, University of Minho, Portugal, jpereira@civil.uminho.pt
José Sena-Cruz, University of Minho, Portugal, jsena@civil.uminho.pt

ABSTRACT
The flexural behaviour of reinforced concrete (RC) slabs strengthened with carbon fibre reinforced polymer (CFRP) laminates is analytically addressed in this work. Analytical approaches are developed for (i) near-surface mounted (NSM), (ii) externally bonded reinforcement (EBR), and the EBR prestressed using (iii) mechanical anchorage (MA) and (iv) gradient anchorage (GA) systems. The analytical results show a good agreement with those from experimental program. Besides, the performance of two existing formulae for predicting the mid-span deflection is assessed, and the performance of the recent fib Bulletin 90 technical report for predicting the ultimate capacity of the strengthened RC slabs is appraised.

KEYWORDS
Strengthened RC slab, CFRP laminate, flexural strengthening, analytical modelling, failure mode.

INTRODUCTION
Carbon fibre reinforced polymer (CFRP) composites can effectively be used to strengthen existing reinforced concrete (RC) structures (Dias et al., 2018). The most common strengthening techniques include externally bonded reinforcement (EBR) and near-surface mounted (NSM) (CEB-FIP, 2019). Additionally, the EBR and NSM can become active techniques , i.e. by prestressing , through mechanical anchorage (MA) or gradient anchorage (GA) systems (Correia et al., 2015), thereby resulting in several cases in the full usage of the fibre reinforced polymer (FRP) strain. Regarding the EBR applied as passive technique, it was found that the premature failure caused by debonding can result in underutilization of the bond constituent materials (Torabian *et al.*, 2020), generally the failure mode (FM) being intermediate crack debonding (ICD) (Bilotta et al., 2013). Furthermore, studies also show that FRP debonding can occur at the end of the strengthened element, known as end debonding (ED) (Ferracuti et al., 2007). On the other hand, the NSM technique can increase the performance of elements that fail in bending (Dias et al., 2018), which makes this technique more reliable. In fact, existing studies show that NSM possesses superior benefits than EBR, e.g. (Barros et al., 2007), (Bilotta et al., 2015), attributed to better FRP-concrete bonding properties (Bianco et al., 2009). The most common FM for NSM is critical diagonal crack debonding (CDCD) or a combination of the CDCD with concrete cover separation (Bilotta et al., 2015).

Regarding the prestressing of the CFRP applied according to EBR (EBR CFRP), the prestressed EBR CFRP combines the benefits of non-prestressed with those of the prestressing (Sena-Cruz et al., 2015). Various studies exist on the use of MA (Garden & Hollaway, 1998) and GA (Michels et al., 2013) as anchorages for prestressed systems. In the former, metallic plates can be placed at the ends of the FRP strips (Sena-Cruz et al., 2015), which will lead to prevention of the premature failure (You et al., 2012). For the case of GA system, it involves a sector-wise accelerated curing of epoxy

adhesive, followed by a segment-wise prestress force release for each heated sector (Michels et al., 2013). Further details can be found in existing literature, e.g. (Correia et al., 2015).

Analytical studies already exist for predicting the flexural behavior of RC elements strengthened with EBR, NSM, GA, and MA systems, e.g., (Badawi & Soudki, 2009), (Mostakhdemin Hosseini et al., 2020), (Rezazadeh et al., 2015) and (Sena-Cruz et al., 2015). However, some aspects have not yet been addressed, for example, existing analytical predictions adopting trilinear moment-curvature relationship generally do not take into account of the effect of the FM nor the prevailing FM. Furthermore, the curvature depends on the neutral axis (NA) location that in turn strongly depends on the FM; however, the curvature determination in most of the existing studies does not include the effects of the predominant FM. Most importantly, no existing analytical predictions that consider using different deflection formulations at a given loading stage to try to examine the effects of each formula on the strengthened element stiffness. This work presents analytical approaches capable of addressing the aforementioned aspects.

METHODS

The moment-curvature relationship for a cross section of an RC slab can be idealized as a trilinear relationship that represents the pre-cracking, post-cracking, and post-yield stages (Rezazadeh et al., 2015). The developed analytical approaches incorporate the conditions that help choose the prevailing FM among the four different failures, namely: concrete crushing (CC), FRP rupture (FR), ED and ICD. To assess the capability of the developed approaches, the results from four different RC slabs (details about the slabs can be found in (Sena-Cruz et al., 2019), and the properties of the material constituents in (Cruz et al., 2021)), previously tested at the laboratory of civil engineering (LEST) of University of Minho, are compared with the analytical results. The main features of the developed analytical approaches are described next.

Constitutive law of the materials

Concrete compressive behavior is assumed linear in both pre- and post-cracking stages up to the yielding of steel. The concrete contribution after the steel yielding (i.e. in the post-yield stage) is simulated by a rectangular stress block mainly governed by a multiplier on the concrete compressive strength to determine the intensity of the stress distribution (k_1) and the ratio of the equivalent rectangular stress block to the neutral axis depth (k_2), as per (CEB-FIP, 2019) recommendations. Furthermore, the tensile behavior of concrete is assumed linear up to the stress where concrete tensile surface starts to have initial cracks as per ACI (ACI-318M-08, 2008).
For the longitudinal steel bars, an elasto-perfectly plastic model is adopted, while the CFRP laminate is modelled as linear up to its ultimate tensile strength.

Moment-curvature relationship

Using section analysis of non-prestressed or prestressed strengthened RC slab, performed based on the strain compatibility and force equilibrium for each of the governing stages, namely pre-cracking, post-cracking, post-yield, and ultimate, the moment-curvature ($M-\varphi$) response was established in each stage. Details on the governing equations for non-prestressed systems can be found in (Dushimimana et al., 2022).

Analytical modelling of RC slabs with prestressing systems

The RC slab prestressed with GA or MA system is modelled using the curvature and moment at pre-cracking (φ_{cr} , M_{cr}), post-cracking (φ_y , M_y), and the moment at post-yield (M_u) stages as provided in Eqs.1-2, Eqs. 3-4, and Eq. 5, respectively.

$$\varphi_{cr} = \varphi_{crp} + |\varphi_{ip}| \quad \text{Eq. 1}$$

$$M_{cr} = \varepsilon_{cct}^{crp} \cdot E_c \cdot b \cdot y_{s^*}^2/3 + \varepsilon_{ccb}^{crp} \cdot E_c \cdot b \cdot (h - y_{s^*})^2/3 + \varepsilon_{st}^{crp} \cdot E_{s2} \cdot A_{s2} \cdot (y_{s^*} - d_{s2}) + \varepsilon_{sb}^{crp} \cdot E_{s1} \cdot A_{s1} \cdot (d_{s1} - y_{s^*}) + \left(\varepsilon_{fb}^{crp} + \varepsilon_{fp}\right) \cdot E_f \cdot A_f \cdot \left(d_f - y_{s^*}\right) \quad \text{Eq. 2}$$

$$\varphi_y = \varphi_{yp} + |\varphi_{ip}| \quad \text{Eq. 3}$$

$$M_y = \varepsilon_{cct}^{yp} \cdot E_c \cdot b \cdot C_{yp}^2/3 + \varepsilon_{st}^{yp} \cdot E_{s2} \cdot A_{s2} \cdot \left(C_{yp} - d_{s2}\right) + \varepsilon_{s1}^{yp} \cdot E_{s1} \cdot A_{s1} \cdot \left(d_{s1} - C_{yp}\right) + \left(\varepsilon_{fb}^{yp} + \varepsilon_{fp}\right) \cdot E_f \cdot A_f \cdot \left(d_f - C_{yp}\right) \quad \text{Eq. 4}$$

$$M_u = A_{s1} \cdot \sigma_{s1} \cdot \left(d_{s1} - k_2 \cdot C_{up}\right) + A_{s2} \cdot \sigma_{s2} \cdot \left(k_2 \cdot C_{up} - d_{s2}\right) + A_f \cdot E_f \cdot \varepsilon_f \cdot \left(h - k_2 \cdot C_{up}\right) \quad \text{Eq. 5}$$

where, $\varepsilon_{cct}^{crp}, \varepsilon_{st}^{crp}, \varepsilon_{sb}^{crp}$ are the strains in concrete top fiber, top steel bar, and bottom steel bar in the pre-cracking stage respectively, and the same notation for strains is used in the post-cracking stage but with the superscript "crp" replaced by "yp". Furthermore, y_{s^*} is the moment of inertia for un-cracked section and d_f is the distance from the center of the CFRP section to the concrete top fiber. The value of ε_c is calculated depending on the type of FM. $d_{s1}$and d_{s2}, A_{s1} and A_{s2}, E_{s1} and E_{s2} are the distance from the center of the bottom and top steel bars to the concrete top fiber, bottom and top steel section area, and bottom and top steel modulus of elasticity, respectively; b is the section width and h is the section height. C_{yp} and C_{up} are the neutral axis depth at yield and ultimate stage, σ_{s1} and σ_{s2} are the stress in bottom and top steel bars, respectively; E_c, E_f, ε_f, and A_f are the elastic modulus of concrete, elastic modulus of FRP, FRP strain, and the FRP section area, respectively.

Formulations for predicting the curvature of the prestressed systems are applied referring to the strain compatibility requirements from a strain profile previously developed by the same authors in (Dushimimana et al., 2022). Based on geometric transformations derived from the above strain profile, the ultimate curvature (φ_u^T), if FM is by FR can be calculated as in Eq. 6 or Eq. 7, or if the FM is by debonding as in Eq. 8 or Eq. 9.

$$\varphi_u^T = \left(\varepsilon_{cct}^{ci} + \varepsilon_{fp}\right)/h + \varepsilon_c/C_{up} \quad \text{Eq. 6}$$

$$\varphi_u^T = \frac{k_2 \cdot \varepsilon_{cu}}{(0.5 \cdot A_f \cdot \sigma_f/k_1 \cdot f_{cm} \cdot b)} \quad \text{Eq. 7}$$

$$\varphi_u^T = \varphi_{ip} + \varepsilon_c\ /C_{up} \quad \text{Eq. 8}$$

$$\varphi_u^T = \frac{k_2 \cdot \varepsilon_c}{(0.5 \cdot A_f \cdot \sigma_f/k_1 \cdot f_{cm} \cdot b)} \quad \text{Eq. 9}$$

where:
ε_{cct}^{ci} and ε_{ccb}^{ci}, f_{cm}, ε_{cu}, ε_{fp}, and C_{up} are top and bottom initial strains in concrete due to prestress, tensile strength of concrete, concrete top fiber ultimate strain, the initial FRP prestrain, neutral axis location at ultimate stage. Furthermore, φ_{ip} and σ_f are determined as shown in (Dushimimana et al., 2022).

Prediction of mid-span deflection
In the present work, the deflection (δ_i) is predicted based on two different existing approaches. The first approach is based on the integration in different loading stages as previously described by (Rezazadeh et al., 2015):

$$\delta_i = \int_{L_i}^{L_i+1} \varphi_i(x) \cdot x \cdot dx \quad \text{Eq. 10}$$

where i can either be $cr, y,$ or u standing for "pre-cracking", "post-cracking" and "post-yield" stages, respectively. Furthermore, x is a variable along the integration region, L_i and L_{i+1} are the corresponding distances of the section boundaries for the region to the support; and φ_i is the curvature. Further details can be found in (Rezazadeh et al., 2015).
The second prediction is based on the calculation of deflection only at determinant section as previously adopted in (Sharaky et al., 2015):

$$\delta_i = \frac{\left(3 \cdot L^2 - 4 \cdot {b_s}^2\right)}{24} \varphi_i \quad \text{Eq. 11}$$

where i and φ_i are as previously defined in Eq. 10. Besides, b_s, L are the shear span length and the span length. It is worth noting that φ_i (Eq. 11) depends on the current concrete top fiber strain and NA depth for non-prestressed systems. It should also be noted that Eq. 11 is only applicable for a 4-point bending test configuration.

Prediction of cracking, yield, and ultimate load
The cracking, yield or failure load based on the maximum bending moment (M_i) can be estimated as (applicable to 4-point bending test configuration):

$$P_i = 4 \cdot M_i/(L - a \cdot L) \quad \text{Eq. 12}$$

where P_i is the load calculated from the corresponding moment (M_i), the subscript i being as previously defined in Eq. 11, and a being the distance from the center of the support to the start of the FRP.

Moment-curvature relationship for RC slabs with prestressed EBR systems
In this work, the formulations capable of incorporating the effect of negative pre-camber on the resulting deflection were developed and proposed as shown in Eqs. 6-9. In fact, for the case when there is a prestressing system, the initial prestress tends to cause a (negative) upward pre-camber and hence a negative curvature. Normally, in experimental tests, the displacements registered in the structural elements are reported without splitting this initial component from the remaining deflections. This can analytically lead to underestimation of the actual deflection that matches with the loading level if the moment (used to calculate the load level) is estimated without including the negative curvature effect. That is, the LVDT considers the first measurement as zero, thereby omitting the effect of the negative camber. This means the measured deflection (by LVDT) is a combination of the negative deflection (from a negative value to zero) and the positive deflection (from zero to a value at failure). However, when plotting the load *vs* deflection curve from experimental test, the deflection (measured by LVDT) is always considered positive, which leads to difficulties during analytical predictions, as the predictions will have to consider both the negative and positive deflections to be able to match with the load recorded during experiment.

Prediction of the prevailing failure mode
The prevailing FM were predicted following the steps shown in Figure 1. Then, the obtained FM were compared with those obtained in the experimental program.

For EBR technique, the FRP failure strain (ε_f) was predicted according to (Balaguru et al., 2009), where the FRP strain at rupture (denoted as ε_{f_FR}) was estimated using Eq. 13, k_m being a multiplier that depends on the FRP unit stiffness, and ε_{fu} being the ultimate FRP strain.

$$\varepsilon_{f\_FR} = k_m \cdot \varepsilon_{fu} \quad \text{Eq. 13}$$

On the other hand, for the failure by ED, the ε_f was estimated as per fib90 (CEB-FIP, 2019), using Eq. 14, in which the FRP strain at ED (ε_{f_ED}) requires both the FRP stress at ED (f_{f_ED}) and elastic modulus (E_f). Furthermore, for the failure by ICD, the E_f and FRP stress at ICD (f_{f_ICD}) were also used to estimate the ε_f at ICD (ε_{f_ICD}) in Eq. 15 as per (CEB-FIP, 2019).

$$\varepsilon_{f\_ED} = f_{f\_ED}/E_f \quad \text{Eq. 14}$$
$$\varepsilon_{f\_ICD} = f_{f\_ICD}/E_f \quad \text{Eq. 15}$$

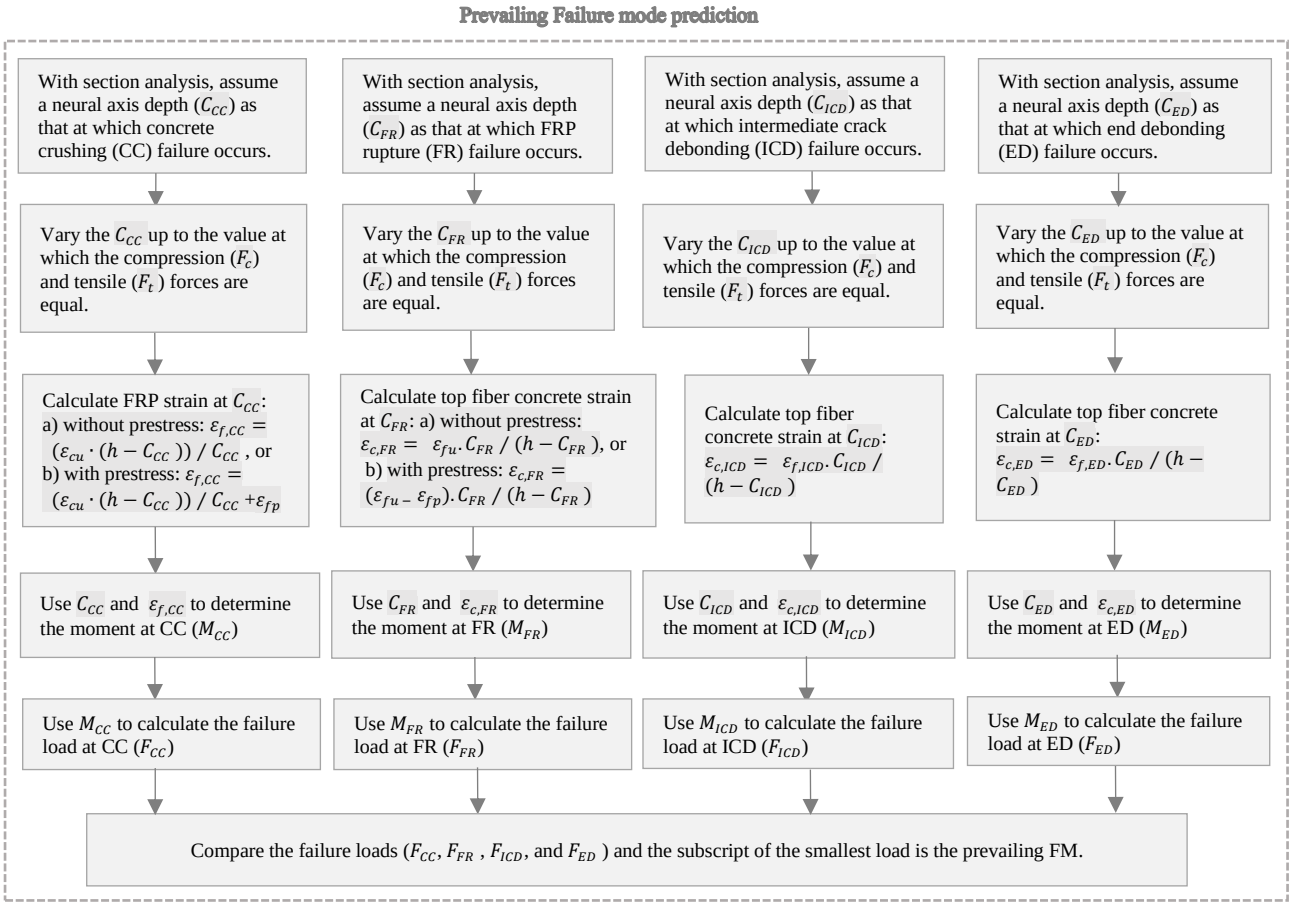

Figure 1: Workflow on the methodology adopted for predicting the prevailing failure mode ($\varepsilon_{fu}, \varepsilon_{cu}, \varepsilon_{fp}, \varepsilon_{f,ED}, \varepsilon_{f,ICD}$, and h are as previously defined).

Hence, based on the above formulations, the ε_f depended on the type of FM as shown in Eq. 16.

$$\varepsilon_f = \begin{cases} \varepsilon_{cu} \cdot (h - C_{us})/C_{us} & if\ failure\ is\ by\ CC \\ \varepsilon_{f\_FR}\ \ from\ Eq.13 & if\ failure\ is\ by\ FR \\ \varepsilon_{f\_ED}\ from\ Eq.14 & if\ failure\ is\ by\ ED \\ \varepsilon_{f\_ICD}\ from\ Eq.15 & if\ failure\ is\ by\ ICD \end{cases} \quad \text{Eq. 16}$$

For NSM technique, the ε_f at FR (ε_{f_FR}) was predicted according to (Barros et al., 2007) using Eq. 17.

$$\varepsilon_{f\_FR} = \left(-32.648 \cdot \rho_{sl,eq} + 0.9606\right) \cdot \varepsilon_{fu} \quad \text{Eq. 17}$$

where, $\rho_{sl,eq}$ and ε_{fu} are the equivalent reinforcement ratio and the FRP ultimate strain, respectively. Besides, the ε_f at ED (ε_{f_ED}) was estimated as per (CEB-FIP, 2019) using Eq. 18.

$$\varepsilon_{f\_ED} = a.\left(\rho_{f,g}\right)^c / \left(E_f A_f\right)^b \quad \text{Eq. 18}$$

where , $\rho_{f,g}$, A_f are the perimeter of the groove and FRP cross-section area, respectively; the regression coefficients are as per fib90 (CEB-FIP, 2019) [i.e., a =252, b = 0.823, and c = 0.66]. Hence, the value of ε_f was estimated depending on the type of FM as per Eq. 19.

$$\varepsilon_f = \begin{cases} \varepsilon_{cu} \cdot (h - C_{us})/C_{us} & if\ failure\ is\ by\ CC \\ \varepsilon_{f\_FR}\ \ from\ Eq.17 & if\ failure\ is\ by\ FR \\ \varepsilon_{f\_ED}\ \ from\ Eq.18 & if\ failure\ is\ by\ ED \end{cases} \quad \text{Eq. 19}$$

For the EBR prestressed using GA and MA systems, the value of ε_f was also predicted depending on the type of FM as shown in Eq. 20.

$$\varepsilon_f = \begin{cases} \varepsilon_{cu} \cdot (h - C_{up})/C_{up} - \varepsilon_{fp} & if\ failure\ is\ by\ CC \\ \varepsilon_{f_{FR}}\ from\ Eq.13 & if\ failure\ is\ by\ FR \\ \varepsilon_{f_{ED}}\ from\ Eq.14\ +\ \varepsilon_{fp} & if\ failure\ is\ by\ ED \\ \varepsilon_{f\_ICD}\ from\ Eq.15\ +\ \varepsilon_{fp} & if\ failure\ is\ by\ ICD \end{cases} \quad \text{Eq. 20}$$

A table was prepared (Table 1) in which all notations, abbreviations, and legends used in the graphs and tables of *results and discussion* section are defined.

Table 1. Notations, abbreviations, and combinations used.

Slab	Deflection	Code	Formulae	Combinations adopted in the legends of graphs and tables
EBR	R, P, RP	FIB*	FIB	FIB_R: FRP FS as per (CEB-FIP, 2019) and deflection as per Eq.10
				FIB_P: FRP FS as per (CEB-FIP, 2019) and deflection as per Eq.11
NSM	P, RP	FIB*	BR	BR_R: FRP FS as per (Barros et al., 2007) and deflection as per Eq.10
				BR_P: FRP FS as per (Barros et al., 2007) and deflection as per Eq.11
				BR_RP: FRP FS as per (Barros et al., 2007) and deflection in both pre/post cracking as per Eq.10 and in post-yield as per Eq.11
MA	R, P, RP	FIB*	BL	BL _R_A: FRP FS as per (Balaguru et al., 2009) and deflection as per Eq.10 and curvature as per Eq.6.
				BL _A_FR: FRP FS as per (Balaguru et al., 2009), curvature as per Eq.6 and FM as FRP rupture.
				BL _WA_FR: FRP FS as per (Balaguru et al., 2009), curvature as concrete top fibre strain/neutral axis, and FM as FRP rupture.
				BL _P_A: FRP FS as per (Balaguru et al., 2009)), deflection as per Eq.11, and curvature as per Eq.6
				BL _R_B: FRP FS as per (Balaguru et al., 2009), deflection as per Eq.10, and curvature as per Eq.7
				BL_P_B: FRP FS as per (Balaguru et al., 2009), and deflection as per Eq.11 and curvature as per Eq.7
				BL _RP_A: FRP FS as per (Balaguru et al., 2009), deflection in both pre/post cracking as per Eq.10 and in post-yield as per Eq.11, and curvature as per Eq.6
				BL _RP_B: FRP FS as per (Balaguru et al., 2009), deflection in both pre/post cracking as per Eq.10 and in post-yield as per Eq.11, and curvature as per Eq.7
GA	R, P	FIB*	FIB	FIB_R_C: FRP FS as per (CEB-FIP, 2019), and deflection as per Eq.10 and curvature as per Eq.8
				FIB_R_WC: FRP FS as per (CEB-FIP, 2019), and deflection as per Eq.10 and curvature as concrete top fibre strain/neutral axis depth
				FIB_P_C: FRP FS as per (CEB-FIP, 2019), and deflection as per Eq.11 and curvature as per Eq.8
				FIB_R_D: FRP FS as per (CEB-FIP, 2019), deflection as per Eq.10 and curvature as per Eq.9
				FIB_R_WD: FRP FS as per (CEB-FIP, 2019), and deflection as per Eq.10 and curvature as concrete top fibre strain/neutral axis depth
				FIB_P_D: FRP FS as per (CEB-FIP, 2019), deflection as per Eq.11 and curvature as per Eq.9.

Notes: R: Eq.10, P: Eq.11, RP is a combination of R and P, the former being used in the pre-and post-cracking stages and the latter being used in the post-yield stage, FIB*: ultimate capacity prediction as per fib90 (CEB-FIP, 2019), FIB: Equation for predicting FRP failure strain as per (CEB-FIP, 2019), FS: failure strain.

RESULTS AND DISCUSSION

Non-prestressed RC slab with EBR or NSM technique

The assessment of the accuracy of the proposed analytical models was performed by comparing analytical predictions with experimental results. Therefore, the experimental program carried out by (Sena-Cruz et al., 2019) was adopted.

The main results for the RC slab strengthened with EBR technique are presented in Figure 2a, in which the legend used is predefined in Table 1. The results show that both Eq. 10 and Eq. 11 can be used as they lead to results that are in a good agreement with those from the experimental program. On the other hand, the force *versus* deflection relation is plotted in Figure 2b (the legend as shown in Table 1) for the case of RC slab strengthened with NSM technique. It can be seen that both attempts lead to good predictions. Particularly, the combination BR_RP leads to slightly better stiffness prediction than BR_P in the post-cracking stage.

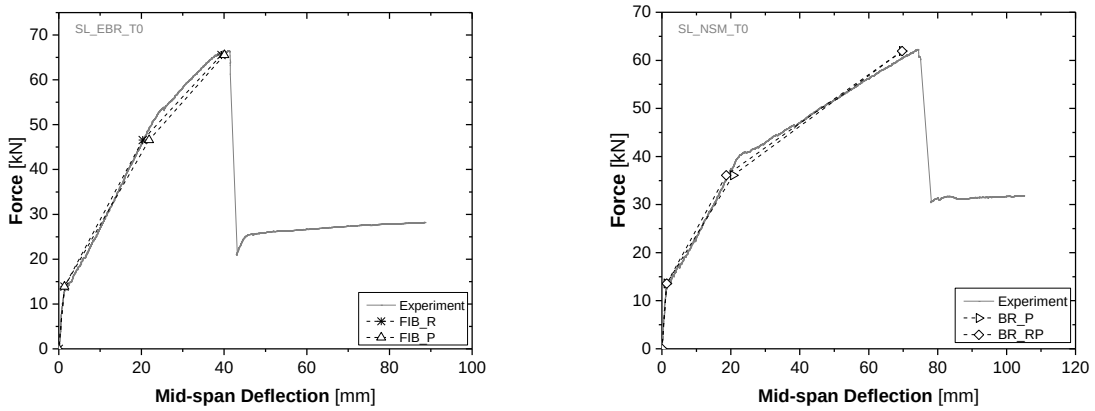

a) EBR technique b) NSM technique

Figure 2: Force *vs.* mid-span displacement of strengthened RC slab – analytical predictions *vs*. experimental results.

RC slab strengthened with EBR prestressed via MA Systems

Effects of proposed curvature formulations

The moment-curvature relationship for RC slab strengthened according to the EBR prestressed using MA systems is presented in Fig. 3a. The legend used in Figure 3a is predefined in Table 1. Both Eq. 6 and Eq. 7 increased the curvature without affecting the moment, thereby incorporating the effect of negative camber. For example, a 32.25% curvature increase was reached when applying Eq. 6 (Fig. 3a). The main purpose of this increase is to encounter the loading level required to bring the concrete and FRP strains back to their initial states (before prestress), as this loading level is included when estimating the failure load (Eq. 12) while the corresponding curvature wouldn't be included if determined by solely dividing the concrete top fiber strain by NA depth.

Load-deflection relationship

The load *vs* deflection relationships after considering the two deflection formulae previously defined in Eq. 10 and Eq. 11, and the two proposed curvature formulae (previously defined in Eq. 6 and Eq. 7) are presented in Fig. 3b-d. The legends used are predefined in Table 1.

It can be noted that the results from the developed analytical approaches are in a good agreement with those from the experimental program. As can be seen from Fig. 3b and Fig. 3c, the combination of BL-P-A or BL-P-B provided better responses than BL-R-A and BL-R-B, which shows that the use of Eq. 11 in the post-yield stage is more preferred than that of Eq. 10. Also, Fig. 3d is used to have an advanced understanding of the combined effect of the two deflection formulations. It can be noted that to have a better stiffness prediction, Eq. 10 or Eq. 11 can be adopted in the pre-cracking stage, Eq. 10 can be adopted in the pre/post-cracking stage, while Eq. 11 can accurately predict the stiffness in post-yield stage that matches with the stiffness from the experimental program (Fig. 3d).

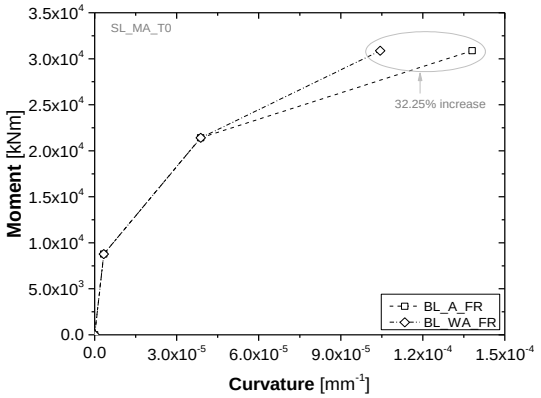

a) Moment *vs* curvature

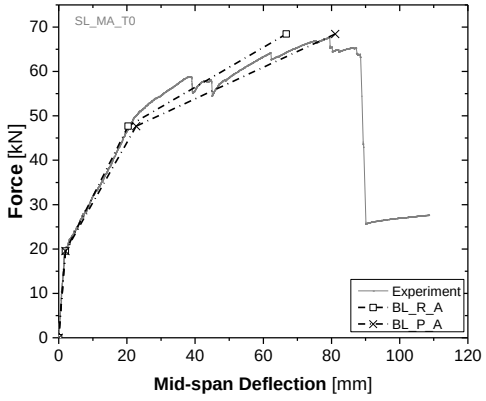

b) Force *vs* mid-span deflection – influence of the deflection estimation approach

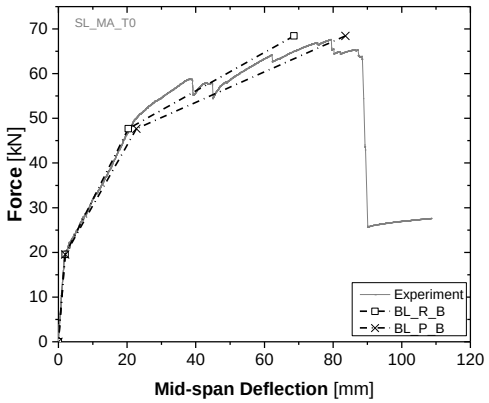

c) Force *vs* mid-span deflection – influence of the deflection estimation approach

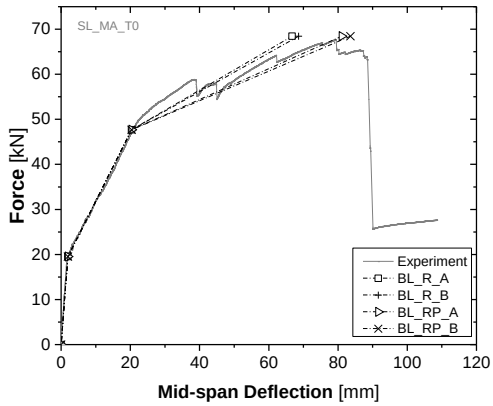

d) Force *vs* mid-span deflection – influence of the deflection estimation approach

Figure 3: Main results for RC slab strengthened according to the EBR MA systems.

RC slab strengthened with EBR prestressed via GA Systems

Load-deflection relationships

The results from the force-deflection relations are presented in Fig. 4, where the legends used are as previously defined in Table 1. It can be noted that the effect of Eq. 8 is insignificant while that of Eq. 9 is more pronounced when predicting the responses in the post-yield stage.

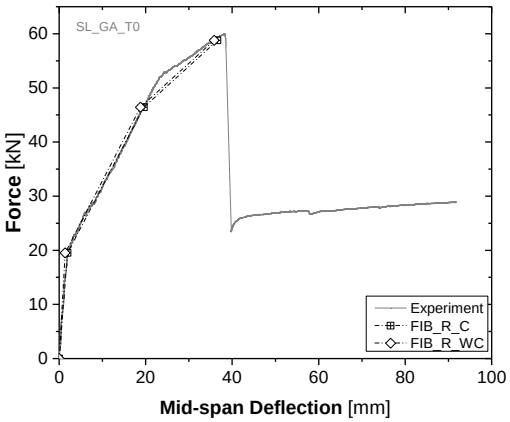

(a)

a) Force *versus* mid-span deflection – influence of the curvature estimation approach

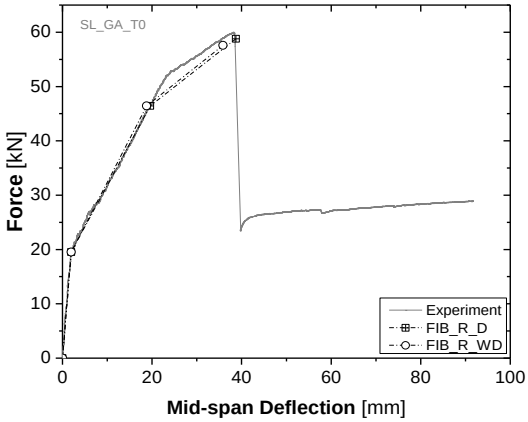

(b)

b) Force *versus* mid-span deflection – influence of the curvature estimation approach

Figure 4: Main results for RC slab strengthened according to the EBR GA systems.

Table 2 summarizes the key results from all strengthened RC slabs. It can be noted that all attempts lead to results that are in a very good agreement with the data recorded during experimental program. That is, most of the analytical predictions lead to results that fall above 90% match with those from experimental program. Furthermore, the results from the prediction of the prevailing FM for EBR, NSM, GA, MA were ICD, FR, ICD, FR failures, respectively, thereby matching well with those observed during experiment, and hence showing the capability of the proposed FM prediction in Fig. 1. Besides, the fact that the predicted FM occur at the load and deflection values (calculated including the proposed curvature formulations) matching with those recorded during experimental program is a clear indication that the developed analytical approach seems reliable. Additionally, FIB (CEB-FIP, 2019) seems reliable for the prediction of the ultimate capacity.

Table 2: Experimental test vs analytical approaches results on the flexural behavior of non-prestressed or prestressed strengthened RC slabs.

Slab	Approach	P_{cr}(kN)	δ_{cr}(mm)	P_y(kN)	δ_y(mm)	P_u(kN)	δ_u(mm)	FM
NSM	Experiment	14.4	2.4	39.9	22.3	62.3	74.4	FR
	BR_R	13.6 (94)	1.4 (56)	36.1 (90)	18.7 (84)	61.9 (99)	61.7 (83)	FR
	BR_P	13.6 (94)	1.4 (56)	36.1 (90)	20.7 (92)	61.9 (99)	69.7 (94)	FR
EBR	Experiment	12.6	1.3	53.2	24.6	66.5	41.2	ICD
	FIB_R	13.9 (110)	1.4 (107)	46.6 (88)	20.3 (83)	65.5 (98)	35.9 (87)	ICD
	FIB_P	13.9 (110)	1.4 (107)	46.6 (88)	22 (89)	65.5 (98)	40.3 (98)	ICD
MA	Experiment	20.4	2.0	49.7	22.2	67.6	79.2	FR
	BL_R_A	19.5 (96)	1.9 (93)	47.7 (96)	20.3 (92)	68.4 (101)	66.7 (84)	FR
	BL _P_A	19.5 (96)	1.9 (93)	47.7 (96)	22.7 (102)	68.4 (101)	81.1 (102)	FR
	BL _R_B	19.5 (96)	1.9 (93)	47.7 (96)	20.3 (92)	68.4 (101)	68.6 (87)	FR
	BL_P_B	19.5 (96)	1.9 (93)	47.7 (96)	22.7 (102)	68.4 (101)	83.6 (106)	FR
GA	Experiment	20.0	2.0	52.0	23.3	59.9	38.2	ICD
	FIB_R_C	19.5 (98)	2.0 (100)	46.4 (89)	19.6 (84)	58.9 (98)	36.5 (95)	ICD
	FIB_P_C	19.5 (98)	2.0 (100)	46.4 (89)	22.0 (94)	58.9 (98)	42.8 (112)	ICD
	FIB_R_D	19.5 (98)	2.0 (100)	46.4 (89)	19.6 (84)	58.9 (98)	37.9 (99)	ICD
	FIB_P_D	19.5 (98)	2.0 (100)	46.4 (89)	22.0 (94)	58.9 (98)	44.9 (118)	ICD

Notations: P_{cr}, P_y, P_u are loads at crack, yield, and ultimate stage respectively; $\delta_{cr}, \delta_y, \delta_u$ are deflections at crack, yield, and ultimate state respectively; FM: failure mode, values in parentheses indicate the difference (in %) between the analytical prediction and the experimental test values

CONCLUSIONS

This work analytically addressed the flexural behavior of RC slabs strengthened with non-prestressed and prestressed CFRP laminates. Comparisons between analytical and experimental results, in terms of force *versus* mid-span deflection and failure modes, were performed. A summary of the key findings is as follows.

1) The developed analytical approaches for predicting the force-deflection curves for both non-prestressed and prestressed systems provided results that are in a good agreement with those from experimental program.
2) For prestressed systems, the formulations for predicting the curvature that incorporates the loading level effects resulting from the negative camber (i.e., the load applied to completely remove the initial negative camber) in both the deflection and load predictions were found to lead to very promising results as compared to the case when the effects are ignored.
3) The two different formulae examined for predicting the mid-span deflection show that the use of one formula at a given loading stage and the other at another loading stage can significantly improve the prediction of the stiffness. In fact, the deflection formula based on the integration is preferable in the pre- or post-cracking stages and for systems failing by

debonding, whereas that based on the determining the deflection at a determinant section is ideal in the post-yield stage.

4) The approach used for determining the failure modes is found to lead to failures that match well with those observed during the experimental program. Taking into account that both the FM and the predicted force vs deflection relationships agree well with the experimental results, it can be thought that the developed analytical approaches are reliable. However, future studies can adopt these approaches using other types of RC slabs in order to have a more advanced understanding of their capabilities. Besides, the section analysis recommended in fib90 (CEB-FIP, 2019) for the ultimate capacity is found reliable.

ACKNOWLEDGEMENT

This work was carried out in scope of the project FRPLongDur POCI-01-0145-FEDER-016900 (FCT PTDC/ECM-EST/1282/2014) and Durable-FRP (PTDC/ECI-EGC/4609/2020) funded by national funds through the Foundation for Science and Technology (FCT) and co-financed by the European Fund of the Regional Development (FEDER) through the Operational Program for Competitiveness and Internationalization (POCI) and the Lisbon Regional Operational Program. This work was partly financed by FCT / MCTES through national funds (PIDDAC) under the R&D Unit Institute for Sustainability and Innovation in Structural Engineering (ISISE), under reference UIDB / 04029/2020. This work is financed by national funds through FCT under grant agreement [DFA/BD/08403/2021] attributed to the first author.

CONFLICT OF INTEREST

The authors declare that they have no conflicts of interest associated with the work presented in this paper.

DATA AVAILABILITY

Data on which this paper is based is available from the authors upon reasonable request.

REFERENCES

ACI-318M-08. (2008). *American Concrete Institute (ACI). Building code requirements for structural concrete.*

Badawi, M., & Soudki, K. (2009). Flexural strengthening of RC beams with prestressed NSM CFRP rods – Experimental and analytical investigation. *Construction and Building Materials*, *23*(10), 3292–3300. https://doi.org/10.1016/j.conbuildmat.2009.03.005

Balaguru, P., Manni, A., & Giancaspro, J. (2009). *FRP Composites for Reinforced and Prestressed Concrete Structures*. Taylor & Francis.

Barros, J. A. O., Dias, S. J. E., & Lima, J. L. T. (2007). Efficacy of CFRP-based techniques for the flexural and shear strengthening of concrete beams. *Cement and Concrete Composites*, *29*(3), 203–217. https://doi.org/10.1016/j.cemconcomp.2006.09.001

Bianco, V., Barros, J. A. O., & Monti, G. (2009). Three dimensional mechanical model for simulating the NSM FRP strips shear strength contribution to RC beams. *Engineering Structures*, *31*(4), 815–826. https://doi.org/10.1016/j.engstruct.2008.12.017

Bilotta, A., Ceroni, F., Nigro, E., & Pecce, M. (2015). Efficiency of CFRP NSM strips and EBR plates for flexural strengthening of RC beams and loading pattern influence. *Composite Structures*, *124*, 163–175. https://doi.org/10.1016/j.compstruct.2014.12.046

Bilotta, A., Faella, C., Martinelli, E., & Nigro, E. (2013). Design by testing procedure for intermediate debonding in EBR FRP strengthened RC beams. *Engineering Structures*, *46*, 147–154. https://doi.org/10.1016/j.engstruct.2012.06.031

CEB-FIP. (2019). *fib90 Bulletin:Externally Applied FRP reinforcement for Concrete structures*.

Correia, L., Teixeira, T., Michels, J., Almeida, J. A. P. P., & Sena-Cruz, J. (2015). Flexural behaviour of RC slabs strengthened with prestressed CFRP strips using different anchorage systems. *Composites Part B: Engineering*, *81*, 158–170. https://doi.org/10.1016/j.compositesb.2015.07.011

Cruz, R., Dushimimana, A., Cabral-fonseca, S., & Sena-cruz, J. (2021). *Durability of Epoxy Adhesives and Carbon Fibre Reinforced Polymer Laminates Used in Strengthening Systems :*

Dias, S. J. E., Barros, J. A. O., & Janwaen, W. (2018). Behavior of RC beams flexurally strengthened with NSM CFRP laminates. *Composite Structures*, *201*(March 2017), 363–376. https://doi.org/10.1016/j.compstruct.2018.05.126

Dushimimana, A., Correia, L., Cruz, R., Pereira, J. M., & Sena-cruz, J. (2022). Analytical approaches for flexural analysis of RC slabs strengthened with prestressed or non-prestressed CFRP laminates. *The 15th International Conference on Fibre-Reinforced Polymers for Reinforced Concrete Structures (FRPRCS-15) & The 8th Asia-Pacific Conference on FRP in Structures (APFIS-2022) 10-14 December 2022, Shenzhen, China*, *December*, 10–14.

Ferracuti, B., Martinelli, E., Nigro, E., & Savoia, M. (2007). Fracture energy and design rules against FRP-concrete debonding. *In: Proc of 8th FRPRCS Conference*, 16–18.

Garden, H. N., & Hollaway, L. C. (1998). An experimental study of the influence of plate end anchorage of carbon fibre composite plates used to strengthen reinforced concrete beams. *Composite Structures*, *42*(2), 175–188. https://doi.org/10.1016/S0263-8223(98)00070-1

Michels, J., Sena-Cruz, J., Czaderski, C., & Motavalli, M. (2013). Structural Strengthening with Prestressed CFRP Strips with Gradient Anchorage. *Journal of Composites for Construction*, 1–46. https://doi.org/10.1061/(ASCE)CC.1943-5614.0000372

Mostakhdemin Hosseini, M. R., Dias, S. J. E., & Barros, J. A. O. (2020). Behavior of one-way RC slabs flexurally strengthened with prestressed NSM CFRP laminates – Assessment of influencing parameters. *Composite Structures*, *245*(February), 112259. https://doi.org/10.1016/j.compstruct.2020.112259

Rezazadeh, M., Barros, J., & Costa, I. (2015). Analytical approach for the flexural analysis of RC beams strengthened with prestressed CFRP. *Composites Part B: Engineering*, *73*, 16–34. https://doi.org/10.1016/j.compositesb.2014.12.016

Sena-Cruz, J., Michels, J., Harmanci, Y. E., & Correia, L. (2015). Flexural strengthening of RC slabs with prestressed CFRP strips using different anchorage systems. *Polymers*, *7*(10), 2100–2118. https://doi.org/10.3390/polym7101502

Sena-Cruz, J., Ricardo Cruz, J., Correia, L., Cabral-Fonseca, S., Michels, J., & Czaderski, C. (2019). Long-term structural and durability performances of reinforced concrete elements strengthened in flexure with CFRP laminates: A research project. *IABSE Symposium, Guimaraes 2019 - Report*, 1006–1014. https://doi.org/10.2749/guimaraes.2019.1006

Sharaky, I. A., Torres, L., & Sallam, H. E. M. (2015). Experimental and analytical investigation into the flexural performance of RC beams with partially and fully bonded NSM FRP bars / strips. *Composite Structures*, *122*, 113–126. https://doi.org/10.1016/j.compstruct.2014.11.057

Torabian, A., Isufi, B., Mostofinejad, D., & Pinho Ramos, A. (2020). Flexural strengthening of flat slabs with FRP composites using EBR and EBROG methods. *Engineering Structures*, *211*(August 2019). https://doi.org/10.1016/j.engstruct.2020.110483

You, Y., Choi, K., & Kim, J. (2012). An experimental investigation on flexural behavior of RC beams strengthened with prestressed CFRP strips using a durable anchorage system. *Composites Part B*, *43*, 3026–3036. https://doi.org/10.1016/j.compositesb.2012.05.030